Simulation and Design of Fluid Catalytic-Cracking Riser-Type Reactors

K. N. Theologos, I. D. Nikou, A. I. Lygeros, and N. C. Markatos
Dept. of Chemical Engineering, National Technical University of Athens, Athens, Greece

Two-phase flow, heat transfer, and reaction in fluid catalytic-cracking riser-type reactors are studied using a 3-D mathematical model. This study was carried out based on the model of Theologos and Markatos, which incorporates a detailed ten-lump reaction kinetics scheme and accounts for gradual feedstock vaporization inside the reactor. Predictions obtained using the new model are compared against industrial reactor operating data. A design study was also carried out to illustrate that the model developed is capable of predicting feed-injector geometry effects on overall reactor performance. It shows that by increasing the number of feed-injection operating nozzles at the bottom of the reactor, selectivity of primary products is improved.

Introduction

Fluid catalytic cracking (FCC) is an industrial process that converts heavy hydrocarbons to lower molecular-weight products and is completed in short-contact-time riser reactors. In a riser reactor the catalyst is pneumatically conveyed by the hydrocarbon vapors from the bottom to the top of a vertical lift line. During this conveying process the catalytic-cracking reactions are completed through the efficient contact of the catalyst with the hydrocarbons.

Evolutionary design changes are constantly being introduced in the FCC process in almost every element involved, including feedstock, catalyst, equipment and products. Additionally, a better understanding of the technologies, particularly fluidization, has brought about major changes.

Riser cracking is established as today's reaction system of choice. The feed-injection area, where preheated liquid gas-oil feedstock is injected inside the reactor and comes into contact with hot regenerated catalyst, is an important section of the reactor. In a typical design of an injector configuration, catalyst flowing at high density comes in contact with a feed-introduction system of high penetration. Catalyst particles are coated with feed as they flow through a feedstock spray and are simultaneously cooled. The intimate contact between feed and catalyst rapidly vaporizes the feed. The increased amount of vapors, due to reaction and vaporization, raise the velocity and lower the density of the flowing system (Murphy, 1992).

The rapid vaporization that takes place leads to a three-phase flow (catalyst, liquid hydrocarbons, and vapor hydrocarbons) at the bottom of the reactor that, after completion of the feedstock vaporization, becomes a two-phase flow (catalyst and vapor hydrocarbons).

Effects of feedstock vaporization and feed-injection configuration have been evaluated in experimental studies in commercial reactors.

Schuurmans (1980) carried out an extensive series of tests in a modern catalytic cracking unit. In the reactor considered, feed was injected in the catalyst stream through three separate nozzles. Trace studies were used to evaluate mixing performance at the bottom of the reactor.

The fact that there were three separate feed-inlet nozzles was initially considered not to be of much importance, assuming that close mixing of feed and catalyst was taking place at the inlet zone. However, this was found not to be the case, since helium trace studies indicated poor mixing in the area.

A typical measured vapor-phase conversion profile along the riser height indicated a local conversion minimum at the bottom of the reactor.

The minimum observed vapor-phase conversion was explained by assuming low evaporation rates and hydrocarbon adsorption in the catalyst related to imperfect mixing of the feed and catalyst.

Cracking rates are affected by temperature distribution, with activation energies indicating that high temperatures shift cracking reactions toward secondary products, such as dry gases and coke. At the bottom of a riser that involves a nonisothermal zone due to a finite mixing time, reaction kinetics affected by temperature distribution becomes a function of nozzle and reactor design (Arbel et al., 1995).

The inlet zone of the reactor is therefore a section where feed-injector geometry affects hydrodynamics and may cause flow inhomogeneities that result in high temperature and concentration gradients. Hot spots, appearing at the inlet zone of a riser reactor, promote cracking reactions to secondary products, thus reducing reactor selectivity.

In summary, cracking reactions in a riser reactor are mainly affected by

- Interphase heat transfer at riser inlet area
- Feedstock vaporization inside the reactor
- Hydrocarbon–catalyst interaction
- Temperature-related reaction kinetics
- Feed-injector complicated geometry.

The simulation of a riser reactor is therefore of considerable importance, since it may lead to a better understanding of the process and efficient equipment design.

Numerous kinetic models have been presented in the literature, taking the form of reaction schemes of varying complexity. Weekman and Nace (1970) proposed a fundamental three-lump kinetics model, while Jacob et al. (1976) developed a more detailed 10-lump kinetics scheme. Reaction schemes of greater complexity may be considered (Svoboda et al., 1994; Baltanas and Froment, 1984; Clymans and Froment, 1984; Quann and Jaffe, 1992), either by increasing the number of lumps, or by using structure-oriented lumping schemes. Reaction kinetics is usually related to riser-outlet temperature; it may also be related to reactor-inlet temperature (i.e., regenerator temperature—Yen et al., 1985) and to the one-dimensional profile of hydrocarbon–catalyst mixture temperature along the riser reactor (Froment and Bischoff, 1990).

Feedstock vaporization inside the reactor, related to interphase heat transfer and feedstock spray atomization, is addressed by Mauleon and Courcelle (1985) and is said to affect critically catalytic cracking unit heat balance. However, no model has yet considered these parameters to assess their influence on reaction kinetics.

In the field of hydrodynamics, theoretical, experimental, and research work is continuously carried out to improve understanding of the complicated hydrodynamics of two-phase flow in vertical transfer lines, which are used not only in riser catalytic cracking but in many industrial applications.

The main assumptions that are usually considered in integrating a kinetics model for yields prediction are one-dimensional flow, single or two-phase flow with constant interphase slip, equal phase temperatures, and instantaneous vaporization inside the reactor. None of these assumptions is valid, at the bottom of the riser reactor, however, since both temperature distribution and mixing time heavily influence nozzle and reactor design.

Despite the progress that has been made in the areas just mentioned no serious efforts have been made to date to combine developments in a single model. A computational fluid dynamics model developed by Theologos and Markatos (1993) assessed the simultaneous influence of the parameters just cited, as well as the impact of feed-injector geometry on hydrodynamics, especially at the bottom of the reactor. Three-dimensional, two-phase flow, with interphase-heat transfer and reaction was considered. Kinetics was described by a three-lump reaction scheme, related to the local 3-D hydrocarbon temperature profile. The main assumption of the model was instant vaporization of feedstock inside the reactor. That research work demonstrated the potential of computational fluid dynamics to serve as a modeling platform not only for the simulation of riser catalytic cracking, but for other complex engineering two-phase problems also (Figure 1).

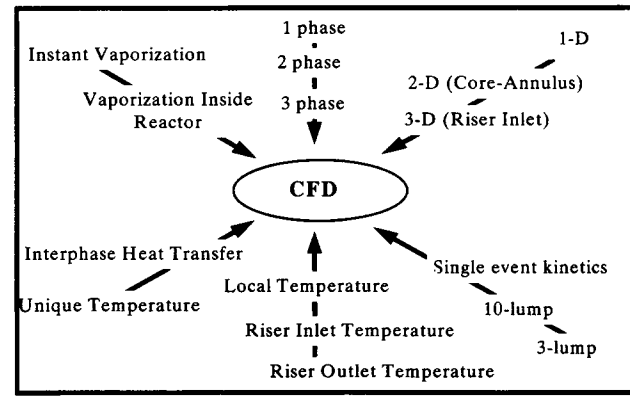

Figure 1. Computational fluid dynamics, a modeling platform for simulation of petroleum catalytic-cracking processes.

In this study, the previously mentioned model is further developed to account for feedstock vaporization inside the reactor and to incorporate a 10-lump reaction kinetics scheme. Model predictions are compared with the industrial reactor operating data, and the model is used to assess the effect of feed-injector geometry on overall reactor performance.

The Physical and Mathematical Model

The main principles of the mathematical model are described in an earlier article (Theologos and Markatos, 1993). The model considers two coexisting and interspersed phases, the vapor hydrocarbons and the solid catalyst. The full set of partial-differential equations governing the 3-D, two-phase flow with heat and mass transfer and with chemical reaction is used. Interphase heat and momentum transfer are accounted for.

Analysis is based on the set of elliptic, partial-differential equations that express the conservation of mass, momentum, and energy in steady 3-D and two-phase flow. The independent variables of the mathematical modeling approach are the three components (θ, r, z) of the polar–cylindrical coordinate system. The main dependent variables are:

- Volume fractions of hydrocarbons and catalyst, R_h and R_c
- Hydrocarbons and catalyst angular momentum, radial, and axial velocities, $(ur)_h$, $(ur)_c$, v_h, v_c, w_h, w_c
- Pressure, p, assumed to be the same for both phases
- Specific enthalpies of hydrocarbons and catalyst, h_h and h_c
- Concentration, y_i, of chemical species i, of hydrocarbons.

The governing partial-differential equations for all variables can be expressed in the following general form:

Table 1. Diffusion Coefficients and Source Terms in Differential Equations (Eq. 1)

φ	Γ_φ	$\int S_\varphi dVol$ (Source Term for the Computational Cell of Volume V)
$R_h = \epsilon$	0	0
$R_c = (1-\epsilon)$	0	0
$(ur)_h$	μ	$-VR_h \frac{\partial P}{\partial \theta} + C_{f,ip} r(u_c - u_h)$
$(ur)_c$	0	$-VR_c \frac{\partial P}{\partial \theta} + C_{f,ip} r(u_h - u_c)$
v_h	μ	$VR_h\left(\frac{\rho_h u_h^2}{r} - \frac{\partial P}{\partial r}\right) + C_{f,ip}(v_c - v_h)$
v_c	0	$VR_c\left(\frac{\rho_c u_c^2}{r} - \frac{\partial P}{\partial r}\right) + C_{f,ip}(v_h - v_c)$
w_h	μ	$VR_h\left(-\rho_h g - \frac{\partial P}{\partial z}\right) + C_{f,ip}(w_c - w_h)$
w_c	0	$VR_c\left(-\rho_c g - \frac{\partial P}{\partial z}\right) + C_{f,ip}(w_h - w_c)$
h_h	μ/Pr	$\dot{q}_{ch} + \dot{q}_{\text{react}}$
h_c	0	$\dot{q}_{hc}$
C_i	μ/Sc	R_i (reaction rate)

$$\frac{\partial}{\partial t}(R_i \rho_i \varphi_i) + \frac{1}{r}\frac{\partial}{\partial r}(rR_i \rho_i v_i \varphi_i) + \frac{1}{r}\frac{\partial}{\partial \theta}(R_i \rho_i u_i \varphi_i) + \frac{\partial}{\partial z}(R_i \rho_i w_i \varphi_i) = \frac{1}{r}\frac{\partial}{\partial r}\left(rR_i \Gamma_{\varphi_i}\frac{\partial \varphi_i}{\partial r}\right) + \frac{1}{r}\frac{\partial}{\partial \theta}\left(R_i \Gamma_{\varphi_i}\frac{\partial \varphi_i}{r\partial \theta}\right) + \frac{\partial}{\partial z}\left(R_i \Gamma_{\varphi_i}\frac{\partial \varphi_i}{\partial z}\right) + S_{\varphi_i}, \quad (1)$$

where φ is the dependent variable; Γ_φ and S_φ are diffusion coefficient and source terms per unit volume for variable φ, respectively; and subscript i refers to the phase in question (hydrocarbons, h, and catalyst, c). For the dependent variables R_h and R_c, $\varphi = 1$ and Eqs. 1 become the phase-continuity equations.

For modeling the steady-state operation of a riser reactor, assuming a 10-lump reaction scheme, twenty differential equations must be solved, for example, for six velocity components, pressure, two volume fractions, two enthalpies, and nine concentrations. The diffusion coefficients, Γ_φ, and source terms, S_φ, in Eq. 1 are given in Table 1. Sources are given as the integral over a control volume. The standard k-ϵ model (Markatos, 1986) may be used for the calculation of turbulence stress terms. In the present study, in order not to further increase the complexity of the simulation, a turbulence viscosity 1,000 times the laminar value, $\mu_{\text{turb}} = 1000\ \mu_{\text{lam}}$, is assumed. The developed model is solved using the SIMPLEST (Spalding, 1980) and IPSA (Spalding, 1977) algorithms that are embodied in the PHOENICS computer program (Spalding, 1981). More details on model development, boundary conditions setting, and numerical solution may be found in Theologos and Markatos (1993).

Feedstock Vaporization Inside the Reactor

Simulation of the feedstock vaporization inside the reactor is addressed and the impact of this phenomenon on the cracking operation and the modeling technique is assessed.

To predict the vaporization phenomenon, the following variables are calculated, mainly at the bottom of the reactor:

- Hydrocarbons temperature, T_h
- Mass fraction of vaporized feed, f
- Hydrocarbons density, ρ_h
- The area where unvaporized feed exists.

All of these variables are related to the specific enthalpy of hydrocarbons, h_h. Since feedstock vaporization inside the reactor is an interphase-heat-transfer-driven process, the enthalpy equations for hydrocarbons and catalyst are solved simultaneously all over the reactor space:

Hydrocarbons

$$\frac{\partial}{\partial t}(R_h \rho_h h_h) + \frac{1}{r}\frac{\partial}{\partial r}(rR_h \rho_h v_h h_h) + \frac{1}{r}\frac{\partial}{\partial \theta}(R_h \rho_h u_h h_h) + \frac{\partial}{\partial z}(R_h \rho_h w_h h_h) = \frac{1}{r}\frac{\partial}{\partial r}\left(rR_h \frac{\lambda}{\bar{c}_{p,h}}\frac{\partial h_h}{\partial r}\right) + \frac{1}{r}\frac{\partial}{\partial \theta}\left(R_h \frac{\lambda}{\bar{c}_{p,h}}\frac{\partial h_h}{r\partial \theta}\right) + \frac{\partial}{\partial z}\left(R_h \frac{\lambda}{\bar{c}_{p,h}}\frac{\partial h_h}{\partial z}\right) + \dot{q}'''_{ch} + \dot{q}'''_{\text{react}}. \quad (2)$$

Catalyst

$$\frac{\partial}{\partial t}(R_c \rho_c h_c) + \frac{1}{r}\frac{\partial}{\partial r}(rR_c \rho_c v_c h_c) + \frac{1}{r}\frac{\partial}{\partial \theta}(R_c \rho_c u_c h_c) + \frac{\partial}{\partial z}(R_c \rho_c w_c h_c) = -\dot{q}'''_{ch}. \quad (3)$$

The mass fraction of vaporized feedstock, f, is calculated as a function of the specific enthalpy of hydrocarbons as follows:

$$f = \begin{cases} 0 & h_h \le \bar{c}_{p,l}(\text{IBP} - T_{\text{ref}}) = h_{\text{IBP}} \\ \dfrac{h_h - h_{\text{IBP}}}{h_{\text{vap}}} & \bar{c}_{p,l}(\text{IBP} - T_{\text{ref}}) < h_h < \bar{c}_{p,l}(\text{IBP} - T_{\text{ref}}) + h_{\text{vap}} \\ 1 & h_h \ge \bar{c}_{p,l}(\text{IBP} - T_{\text{ref}}) + h_{\text{vap}} = h_{\text{IBP}} + h_{\text{vap}} \end{cases} \quad (4)$$

In the temperature range between the feedstock initial (IBP) and final (FBP) boiling points, hydrocarbon temperature, T_h, is calculated as a function of the mass fraction of vaporized feedstock, f. The relation used is based on the distillation curve (ASTM D-1160) of a typical Hellenic Aspropyrgos Refinery feedstock, which is converted at hydrocarbon partial pressure conditions inside the reactor:

$$T_h = f(f). \quad (5)$$

For the given reactor temperature operating range, hydrocarbon temperature, T_h, is calculated as a function of hydrocarbon specific enthalpy, h_h, as follows:

Table 2. Vaporization Simulation Data

Reactor dimensions	
Height	30 m
Cross-section area	1.2 m^2
Number of nozzles	8
Nozzles inclination	60°
Physical properties	
Hydrocarbons	
Density (gas)	7.2 kg/m^3
Density (liquid)	900 kg/m^3
Laminar viscosity	2×10^{-5} Pa·s
Thermal conductivity	0.07 W/(m·K)
Specific heat (gas)	3,350 J/(kg·K)
Specific heat (liquid)	2,670 J/(kg·K)
Heat of vaporization	191 kJ/kg
Endothermic heat of reaction	465 kJ/kg feed
Feedstock IBP	533 K
FBP	803 K
Catalyst	
Particle density	1,300 kg/m^3
Specific heat	1,110 J/(kg·K)
Particle diameter	60 μm
Interphase heat-transfer coefficient	$Nu_p = 0.03\ Re_p^{1.3}$

tive to the hydrocarbon density calculation, two different cases were studied: a. hydrocarbon density equal to vapor density; b. hydrocarbon density changes along with vaporization.

The reactor dimensions and physical properties, as well as the boundary conditions for the simulation considered, are presented in Tables 2 and 3, respectively. Three-dimensional predictions were obtained using the introduced vaporization scheme, and the results of both cases are presented over the first 10 m of the reactor.

For the two cases described earlier, Figure 2 illustrates the predicted vaporized fraction of the feedstock, x_h, at a horizontal plane at the bottom of the reactor. Predictions of x_h for both cases at the vertical plane passing from the feed-injection point are presented in Figure 3. Figure 4 illustrates the predicted axial distribution of the vaporized fraction of the feedstock for cases a and b. It is predicted that complete feedstock vaporization takes place over the first 5 to 3 m of the riser reactor, depending on the hydrocarbon-density-calculation assumption used. As far as prediction of yields at the reactor exit is concerned, gasoline and secondary products values are not affected by the vaporization scheme used.

$$T_h = \begin{cases} T_{\text{ref}} + \dfrac{h_h}{\bar{c}_{p,l}} & f = 0 \quad T_h < \text{IBP} \\ f(f) & 0 \le f \le 1 \quad \text{IBP} \le T_h \le \text{FBP} \\ \text{FBP} + \dfrac{h_h - h_{\text{vap}} - \bar{c}_{p,l}(\text{IBP} - T_{\text{ref}})}{\bar{c}_{p,g}} & f > 1 \quad T_h > \text{FBP}. \end{cases} \tag{6}$$

The hydrocarbon vapor–liquid mixture density, ρ_h, is calculated as a weighted average of gaseous and liquid hydrocarbon densities:

$$\rho_h = x \cdot \rho_g + (1 - x) \cdot \rho_l. \tag{7}$$

From the computational point of view, rapid density variations at the bottom of the reactor lead to a slow algorithm convergence. To assess the sensitivity of the algorithm rela-

Table 3. Boundary Conditions

Hydrocarbons inlet	
At $z = 0$, $r = R$, $\theta = 0$, and at $z = 0$, $r = R$, $\theta = \pi/4$ (i.e., at nozzles' exit)	
Mass flow rate:	$F_h = 42.7/8/2$ kg/s = 2.67 kg/s
Velocity:	$w_h = 50$ m/s * sin 60° = 43.3 m/s
	$v_h = 50$ m/s * cos 60° = 25 m/s
	$(ur)_h = 0$ m/s
Vaporized feedstock:	$x_h = 0$ (v/v)
Density:	Case a: $\rho_h = \rho_g$
	Case b: $\rho_h = \rho_l$
Specific enthalpy:	$h_h = 0$ J/kg ($T_{\text{ref}} = T_{\text{inlet}} = 473$ K)
Lumps concentration:	
Gasoil:	1 (w/w)
Gasoline:	0 (w/w)
Secondary products:	0 (w/w)
Catalyst Inlet	
At $z = 0$, $r = [0, R]$, $\theta = [0, \pi/4]$	
Mass flow rate:	$F_c = 140/8$ kg/s = 17.5 kg/s
Specific enthalpy:	$h_c = 1{,}110$ J/(kg·K) * 1,000 K = 1.11×10^6 J/kg ($T_{\text{ref}} = 0$ K)

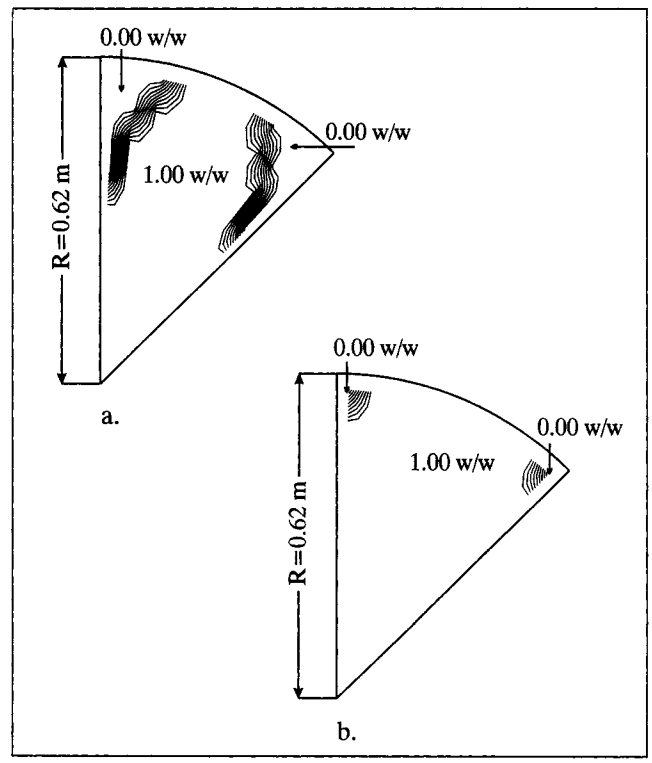

Figure 2. Vaporized fraction of feedstock at the bottom of the reactor.

Case a: Hydrocarbon density equal to vapor density; Case b: Hydrocarbon density changes along with vaporization.

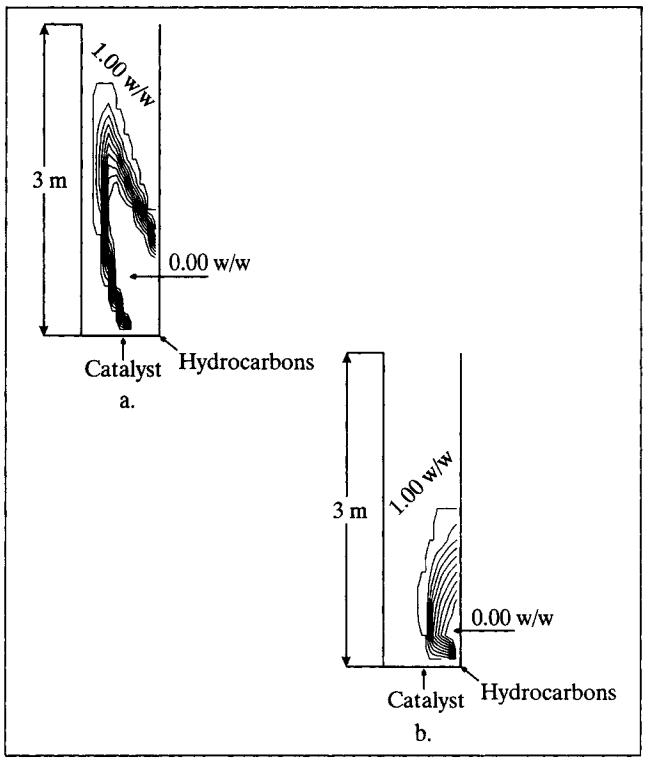

Figure 3. Vaporized fraction of feedstock at vertical planes passing from the injection points.

Case a: Hydrocarbon density equal to vapor density; Case b: Hydrocarbon density changes along with vaporization.

From the computational point of view, convergence considering "hydrocarbon density change along with vaporization" is five times slower than convergence considering "hydrocarbons density equal to vapor density," and therefore the introduction of the assumption "hydrocarbons density equal to vapors density," reduces considerably computational time without affecting yields predictions.

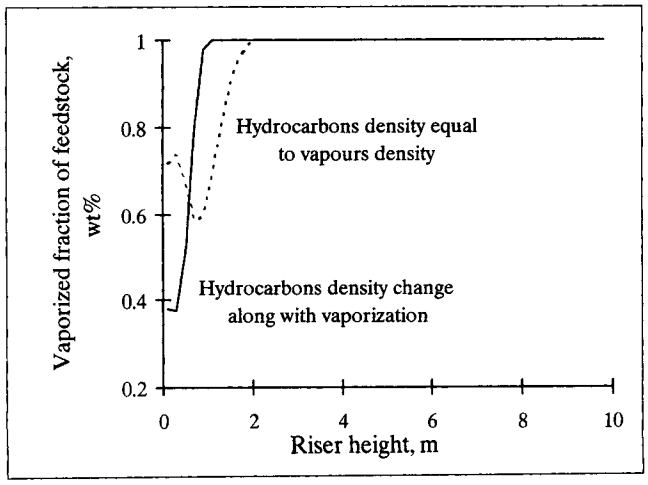

Figure 4. Vaporized fraction of feedstock vs. riser height.

Table 4. Predicted vs. Actual Variables at the Exit of the Reactor

Variables	Predicted	Actual
ΔP (kg/cm^2)	0.14	0.17
T_{out} (°C)	509	517
Heavy fuel oil (wt. %)	8.5	7.3
Light fuel oil (wt. %)	20.5	19.9
Gasoline (wt. %)	47.7	48.0
Dry gases + coke (wt. %)	23.3	24.8

Introduction of the Ten-Lump Kinetic Model

Mobil's ten-lump kinetic model (Jacob et al., 1976) is incorporated into the hydrodynamic model, and predictions are compared with industrial riser-reactor operating data. The Hellenic Aspropyrgos Refinery (HAR) reactor is considered. The kinetics model considers the following lumps:

P_h = paraffin molecules (heavy fractions)
N_h = naphthenic molecules (heavy fractions)
As_h = aromatic substituent groups (heavy fractions)
Ar_h = carbon atoms among aromatic groups (heavy fractions)
P_l = paraffin molecules (light fractions)
N_l = naphthenic molecules (light fractions)
As_l = aromatic substituent groups (light fractions)
Ar_l = carbon atoms among aromatic groups (light fractions)
G = gasoline
C = dry gases + coke

where, subscript l refers to fractions boiling between 221°C and 343°C (light fractions), while subscript h refers to heavy fractions (boiling point > 343°C).

Predicted values at the exit of the reactor are summarized in Table 4. The sum of heavy fractions is reported as heavy fuel oil (HFO), while light fractions are reported as light fuel oil (LFO). Figure 5 illustrates the predicted distribution of product yields along the riser height.

Design Study

The ability of the model to evaluate the effect of feed-injector geometry on overall reactor performance is assessed. More specifically, the effect of the number of feed-injection operating nozzles on overall reactor performance is evaluated. Two 3-D simulations are presented that consider 3 and

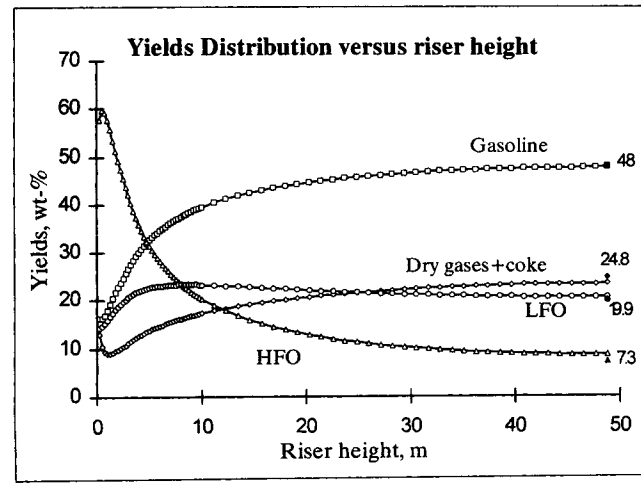

Figure 5. Yields distribution vs. riser height.

12 nozzles operating at the bottom of the reactor, injecting feed toward the center of the reactor at an angle of 60° with the horizon.

The computational domain for the cases considered is presented in Figure 6. The distributions of the main design variables (i.e., velocities, catalyst volume fraction, temperature, primary, and secondary product) at the bottom of the riser reactor are presented in Figures 7 to 11, while Figures 12 and 13 show primary and secondary product yield distribution along riser height.

The sequence of main-variable distribution graphs illustrates the effect of hydrodynamics at the bottom of the riser on reactor performance. As indicated by the axial velocity distribution, high upward velocities are observed near the feed injection nozzles, while low acceleration or even back mixing occurs at the area between the nozzles. At the stagnant/low acceleration area, low feed penetration in the catalyst phase is predicted, leading to higher flowing system densities, and consequently to higher temperatures. Predicted back mixing finally affects cracking rates, leading to a local yield minimum at the bottom of the reactor, as presented in Figures 12 and 13.

A conversion minimum was also measured by Schuurmans (1980) in a commercial catalytic cracking unit that was related to feedstock adsorption in catalyst particles. Although this minimum was not related to temperature distribution as considered in the present study, it was said to be an effect of imperfect mixing of feed and catalyst, which led to the same conclusion with the present modeling approach.

By increasing the number of nozzles, better acceleration is

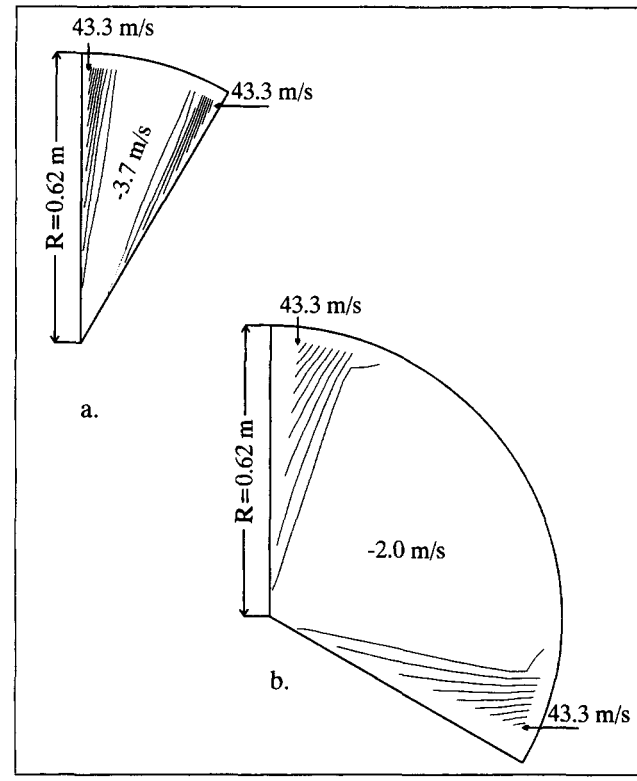

Figure 7. Hydrocarbon axial velocity distribution at the bottom of the reactor ($z = 0.1$ m).

(a) Case 1: 12 nozzles operate at the bottom of the reactor; (b) Case 2: 3 nozzles operate at the bottom of the reactor.

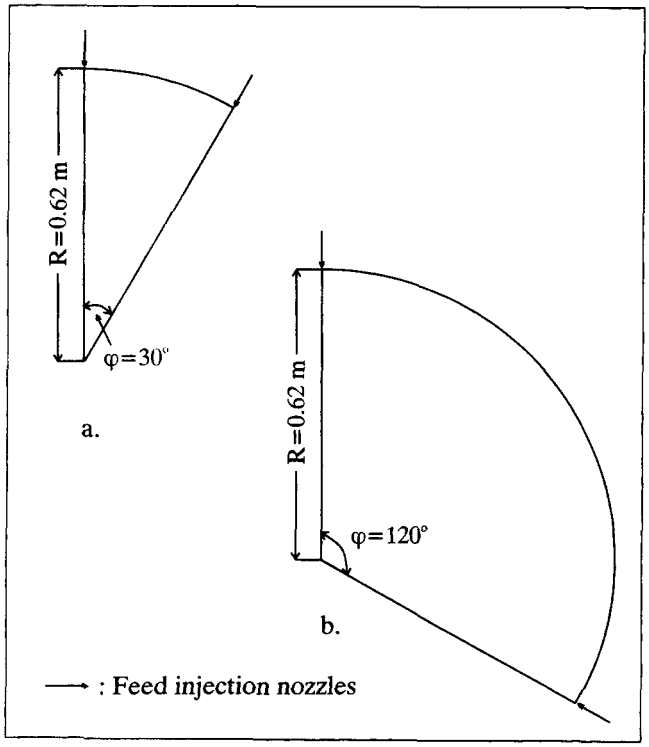

Figure 6. Computational domain at the bottom of the reactor.

(a) Case 1: 12 nozzles operate at the bottom of the reactor; (b) Case 2: 3 nozzles operate at the bottom of the reactor.

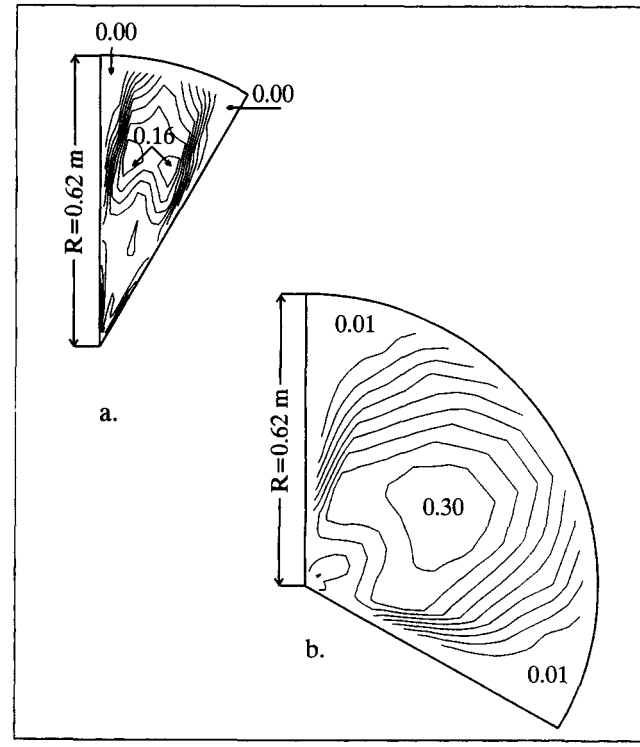

Figure 8. Catalyst volume fraction distribution at the bottom of the reactor ($z = 0.1$ m).

(a) Case 1: 12 nozzles operate at the bottom of the reactor; (b) Case 2: 3 nozzles operate at the bottom of the reactor.

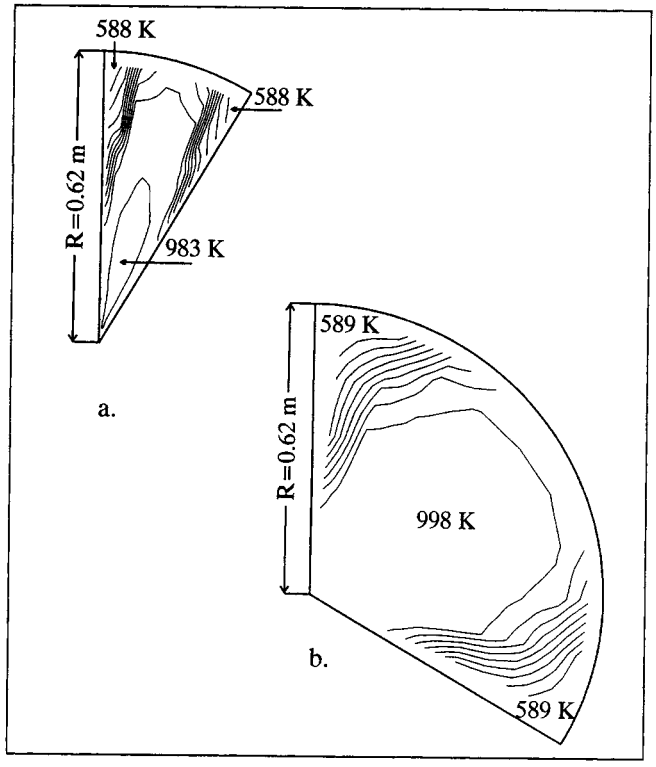

Figure 9. Hydrocarbons temperature distribution at the bottom of the reactor ($z = 0.1$ m).

(a) Case 1: 12 nozzles operate at the bottom of the reactor;
(b) Case 2: 3 nozzles operate at the bottom of the reactor.

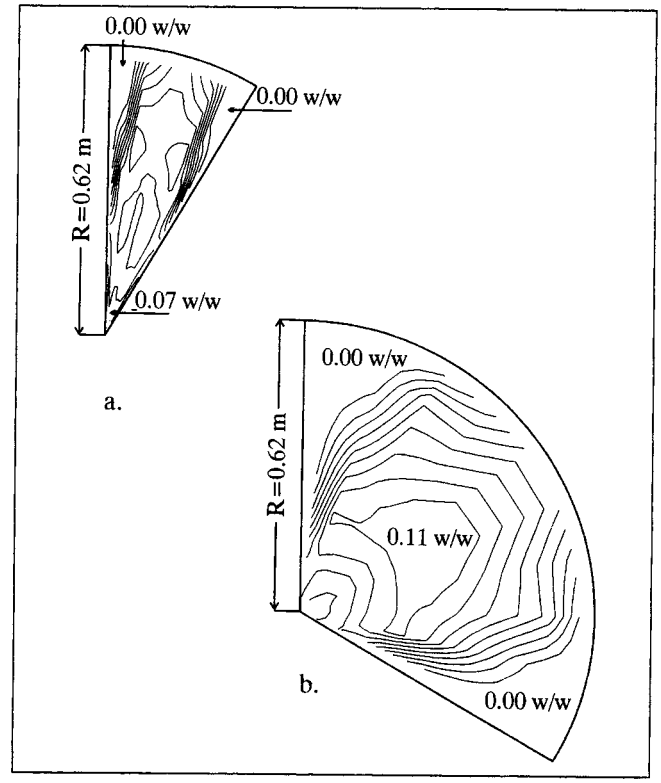

Figure 11. Dry gases+coke distribution at the bottom of the reactor ($z = 0.1$ m).

(a) Case 1: 12 nozzles operate at the bottom of the reactor;
(b) Case 2: 3 nozzles operate at the bottom of the reactor.

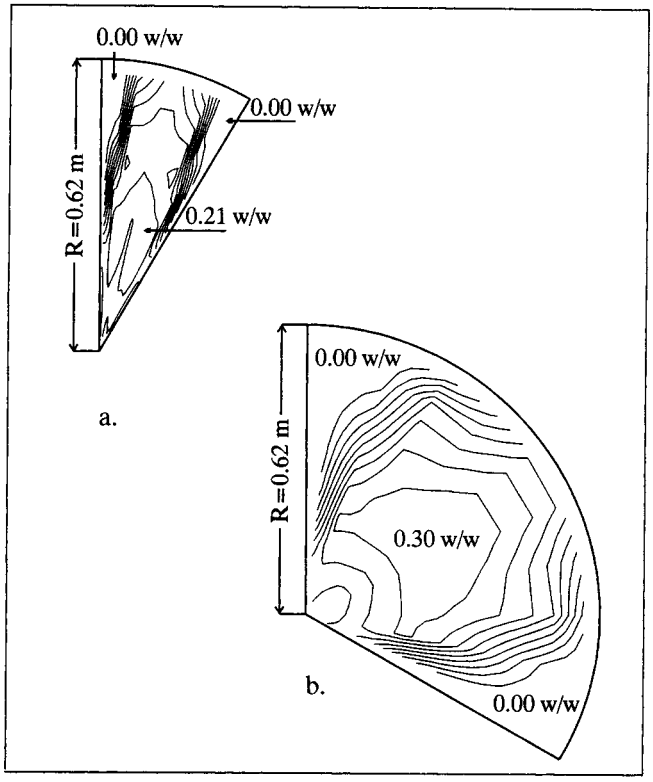

Figure 10. Gasoline concentration distribution at the bottom of the reactor ($z = 0.1$ m).

(a) Case 1: 12 nozzles operate at the bottom of the reactor;
(b) Case 2: 3 nozzles operate at the bottom of the reactor.

achieved, reducing the stagnant region between the two nozzles and leading to lower catalyst volume fractions. The number of high-temperature areas is reduced and lower temperature gradients are observed. Since extreme temperature values tend to promote cracking rates to secondary products, better mixing eliminates "hot spots" and reduces secondary product yields.

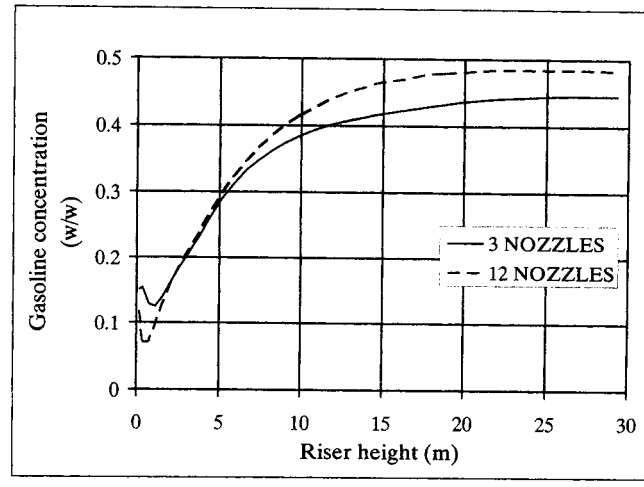

Figure 12. Effect of the number of nozzles on gasoline yields.

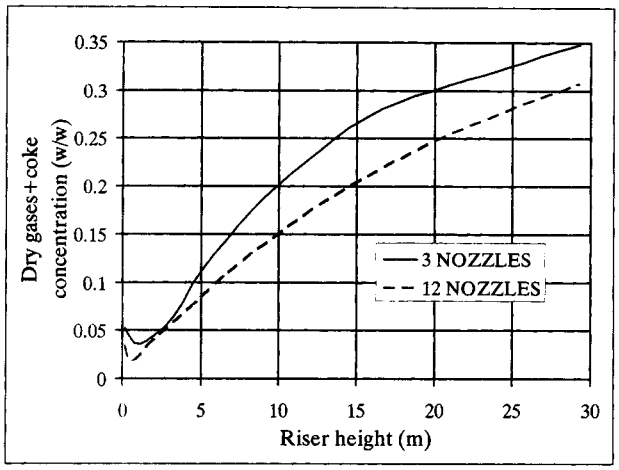

Figure 13. Effect of the number of nozzles on dry gases +coke yields.

Main variables predictions at the bottom and the exit of the reactor are presented in Table 5. Predictions show that by increasing the number of nozzles operating at the bottom of the reactor from 3 to 12:

- Better mixing at the bottom of the reactor is achieved.
- Catalyst volume fraction at the bottom of the reactor is reduced.
- Temperature at the bottom of the reactor is reduced.
- The cracking rate at the bottom of the reactor is reduced.
- Selectivity to secondary products at the bottom of the reactor is reduced.
- Secondary products at the exit of the reactor are reduced and gasoline yield is increased, thus improving selectivity.

Conclusions

A 3-D hydrodynamic model has been developed that predicts two-phase flow, heat transfer, and reaction in FCC, riser-type reactors. The model is enhanced with the introduction of a feedstock vaporization scheme to predict that feedstock vaporizes completely at the first 1.5 to 3 m of the reactor. A 10-lump kinetic model was introduced to describe cracking reactions, and predictions are compared with industrial riser reactor measurements.

A design study was carried out to illustrate that the model is capable of predicting feed-injector geometry effects on overall reactor performance. It is predicted that, by increasing the number of feed-injection operating nozzles at the bottom of the reactor, selectivity to primary products is improved. The developed model can serve as a design tool in FCC, riser-type reactors, since it may predict the main hydrodynamics, heat-transfer, and reaction aspects of this process, as well as conversion and selectivity trends affected by geometrical configuration parameters.

Table 5. Main Variables at the Bottom ($z = 0.1$ m) at the Exit ($z = 30$ m) of the Reactor

	T_h (K)	Conversion (% w/w)	Gasoline (% w/w)	Dry Gases + Coke (% w/w)
At the bottom of the reactor				
3 nozzles	877	20.4	15.1	5.3
12 nozzles	864	15.2	11.7	3.4
At the exit of the reactor				
3 nozzles	750	79.9	44.4	35.5
12 nozzles	751	79.7	48.2	31.5

Acknowledgments

This work was performed in the framework of a JOU2-CT92-122 EEC contract. The financial support of the EEC (Directorate General XII) is gratefully acknowledged. The computations were performed using the PHOENICS computer program of CHAM, Ltd., Wimbledon, London, UK.

Notation

$C_{f,ip}$ = interphase friction coefficient
C_i = concentration of lump i (w/w)
$\bar{c}_{p,g}$ = mean specific heat of vapor hydrocarbons, J/kg·K
$\bar{c}_{p,h}$ = mean specific heat of hydrocarbons, J/kg·K
$\bar{c}_{p,l}$ = mean specific heat of liquid hydrocarbons, J/kg·K
h_{IBP} = specific enthalpy of hydrocarbons at IBP of feedstock, J/kg
h_{vap} = heat of vaporization, J/kg
Pr = Prandtl number
$\dot{q}'''_{ch}$ = interphase heat transfer per unit volume from catalyst to hydrocarbons, J/m^3·s
$\dot{q}'''_{hc}$ = interphase heat transfer per unit volume from hydrocarbons to catalyst, J/m^3·s
$\dot{q}'''_{react}$ = heat of reaction per unit volume, J/m^3·s
R_i = reaction rate for chemical lump i (kg/s)
Sc = Schmidt number
T_{ref} = reference temperature, K
x = hydrocarbons vaporized volume fraction (vol/vol)
$\epsilon = R_h$ = lift-line voidage
λ = thermal conductivity, W/m·K
ρ_g = density of gaseous hydrocarbons, kg/m^3
ρ_l = density of liquid hydrocarbons, kg/m^3

Subscripts

g = hydrocarbons (gaseous phase)
l = hydrocarbons (liquid phase)

Literature Cited

Arbel, A., Z. Huang, I. H. Rinard, R. Shinnar, and A. V. Sapre, "Dynamic and Control of Fluidized Catalytic Crackers. 1. Modeling of the Current Generation of FCC's," *Ind. Eng. Chem. Res.*, **34**, 1288 (1995).

Baltanas, M. A., and G. F. Froment, "Computer Generation of Reaction Networks and Calculation of Products Distribution in the Hydroisomerization and Hydrocracking of Paraffins on Pt-Containing Bifunctional Catalysts," *Comput. Chem. Eng.*, **9**(1), 71 (1985).

Clymans, P. J., and G. F. Froment, "Computer-generation of Reaction Paths and Rate Equations in the Thermal Cracking of Normal and Branched Paraffins," *Comput. Chem. Eng.*, **8**(2), 137 (1984).

Froment, G. F., and K. B. Bischoff, *Chemical Reactor Analysis and Design*, 2nd ed., Wiley, New York, p. 586 (1990).

Jacob, S. M., B. Gross, S. E. Voltz, and V. W. Weekman, "A Lumping and Reaction Scheme for Catalytic Cracking," *AIChE J.*, **22**(4), 701 (1976).

Markatos, N. C., "The Mathematical Modelling of Turbulent Flows," *Appl. Math. Model.*, 190 (1986).

Mauleon, J. L., and J. C. Courcelle, "FCC Heat Balance Critical for Heavy Fuels," *Oil Gas J.*, 64 (1985).

Murphy, J. R., "Evolutionary Design Changes Mark FCC Process," *Oil Gas J.*, 49 (1992).

Quann, R. J., and S. B. Jaffe, "Structure-Oriented Lumping: Describing the Chemistry of Complex Hydrocarbon Mixtures," *Ind. Eng. Chem. Res.*, **31**, 2483 (1992).

Schuurmans, H. J. A., "Measurements in a Commercial Catalytic Cracking Unit," *Ind. Eng. Chem. Process Des. Dev.*, **19,** 267 (1980).
Spalding, D. B., *Turbulent Buoyant Convection*, N. Afgan and D. B. Spalding, eds., Hemisphere, Washington, DC, p. 569 (1977).
Spalding, D. B., "Mathematical Modelling of Fluid Mechanics, Heat Transfer and Chemical Reaction Processes; A Lecture Course," Rep. HTS/80/1, Imperial College, London (1980).
Spalding, D. B., "A General Purpose Computer Program to Multi-Dimensional One or Two-Phase Flow," *Mathematics and Computers in Simulation*, **XIII**, p. 267 (1981).
Svoboda, G. D., E. Vynckier, B. Debrabandere, and G. F. Froment, "Single-event Rate Parameters for Paraffin Hydrocracking on a Pt/US-Y Zeolite," *Ind. Eng. Chem. Res.*, **34,** 3793 (1995).
Theologos, K. N., and N. C. Markatos, "Advanced Modelling of Fluid Catalytic Cracking Riser-Type Reactors," *AIChE J.*, **39**(6), 1007 (1993).
Weekman, V. W., and D. M. Nace, "Kinetics of Catalytic Cracking Selectivity in Fixed, Moving and Fluid Bed Reactors," *AIChE J.*, **16**(3), 397 (1970).
Yen, L. C., R. E. Wrench, and C. M. Kuo, "FCCU Regenerator Temperature Effects Evaluated," *Oil Gas J.*, 87 (1985).

Manuscript received Apr. 29, 1996, and revision received Aug. 7, 1996.